Nigerian Journal of Theoretical and Environmental Physics (NJTEP)
ISSN Print: 3026-9601
DOI: https://doi.org/10.62292/njtep.v2i2.2024.47
Volume 2(2), June 2024

Transient Models of a Photophoretically Filtering Structure in the Stratosphere

Hadiza Nass Sani

Institute of Education, Ahmadu Bello University, Zaria, Nigeria

*Corresponding author's email: hadizanass@yahoo.com

ABSTRACT

The stratosphere has very little convection and tends to trap any dust and gases that enter this region from the atmosphere. This study suggests how dust and particles can be filtered from the stratosphere by a 2-plated parallel-walled infinite rotatable, levitating vertical/horizontal channel (preferably) perforated with holes which have pockets on the cooler upper wall for collecting particles. A movement of particles by light called photophoresis, is caused by the radiative warming layer of a sandwich structure. Collisions of gases with surface of structure and thermal gradients between the two thin plates will also deflect particles. Equations of momentum and energy are solved using an implicit finite difference scheme while exact solutions are presented for steady state dimensionless velocity, concentration and temperature for a fully developed flow. Heat and mass transfer characteristics of parameters like time are displayed graphically. Combined photophoretic and thermophoretic effect on water particles ($Sc = 0.6$) is negligible when compared to soot or dust particles ($Sc = 600$).

Keywords:
Heat and mass transfer,
Photophoresis,
Stratosphere,
Parallel plates,
Conductive boundary conditions.

INTRODUCTION

The stratosphere, located above troposphere, is derived from the Greek word '*stratum*' meaning 'layer' – referring to the layer's stratified is non-convective nature. Gases and dust form volcanic eruptions, ballons, space crafts, meteorological interplanetary particles remain trapped there for months or longer, (NASA, 2024). Temperature increases with height from c. –60^{O}C (lower stratosphere) to c.0°C at c.50 km ASL (stratopause), It contains small amounts of ozone (Ozone Layer) – absorbs ultraviolet (UV) solar radiation, causing warming of stratosphere and has extremely dry layer with no weather (stable conditions due to cold air below), very little convection takes place, traps any and all gases from atmosphere. Most meteorites entering the atmosphere burn out above the stratosphere (National Weather Service Shreveport, 2024).

Submicron aerosol particles are also released upon combustion of fuels and in food and chemical industries and found in dust. Aerosols are suspensions of tiny, sometimes spherical particles in air or gaseous mediums. They can be suspended in the atmosphere, factories, human lungs, buildings and confined spaces which makes their motion, deposition and settling important to Health, hazard control, pollution control, engineering and safety research.

A levitating alumina filtration device deployed in the stratosphere is proposed. The Turbulent forces make deployment of this photophoretic two-panel device from aircraft implausible. Deployment might be achieved using weather balloon technology that can easily lift 1 kg to the stratosphere. Devices could be fabricated and transported while attached to a carrying frame with piezoelectrically controlled latches or fusible wax joints. In heat transfer, free and forced convection exists when we have buoyancy forces and a pressure force respectively, when the two forces exist together, this situation is known as mixed convection. Rahman & Carey (1986) examined a horizontal mixed convective flow in the region of a hot vertical plate. Bouhdjar and Harhad (2002) presented a computational study of a mixed convection in a fluid tank considering effects of parameters on stratification. Ngyuyen *et al*. (2004) presented a study of unsteady mixed convection flow in a pipe of vertical length. Popa *et al.* (2014) analysed transient vertical duct flow with mixed convection involving nanofluids. Xu and Pop (2012) studied mixed convection flow in a vertical conduit of nanofluids. Barletta *et al*. (2005) analysed two flows in a vertical channel having mixed convection. They discussed the classical problem of the fully developed mixed convection flow with frictional heat generation in a vertical channel bounded by isothermal plane walls

having the same temperature. Saleh *et al.* (2013) studied a chemically reacting mixed convection flow in an upright channel. Sun *et al*. (2012) and Al-Amri (2021) studied mixed convection flows in upright channels in a chemically reactive flow and an aiding flow of a nanofluid respectively. Singh *et al.* (1996), Paul *et al.* (1996), Jha and Ajibade (2010), Jha (2001) and Das *et al.* (2016) considered vertical natural convective flows in transient states.

In the event of the mixing of a couple or more of particles of dust and a geothermal gradient (direction showing rate of temperature change), we observe grey/black gases of particles moving away from the hot plate. When particles are heated, they gain kinetic energy and push the large slow particles towards the cold plate with a force referred to as the thermophoretic force, leaving an empty region free of particles. Messerer *et al.* (2003) experimentally observed thermophoresis in soot deposition from diesel engine exhaust systems. Sasse *et al.* (1994) developed a particle filter that uses thermophoresis and natural flow for transportation, analyzing this migration in concentric pipes and between parallel walls. Mensch and Cleary (2019) provided calculations of estimations predicting deposition of soot deposition. Tsai and Lu (1995) gave an illustration and evaluation of a parallel-plated precipitator using thermophoresis. Effects of natural convection in a thermophoretic flow have been investigated by Epstein et.al. (1985) and Postelnicu (2007), Wang and Jayarag (1999). Grosan *et al*. (2009) presented a theoretical and numerical analysis of the transport of submicron particles in thermophoretic mixed convection flows bounded by two vertical walls. In the paper of Magyari (2009), a detailed analytic approach to the study of Grosan *et al*. (2009) was presented. A transient analysis of thermophoretic particle movement and deposition under nanofluid-pool boiling conditions has been presented by Karthikeyan et al. (2020). Jha and Sani (2021) investigated unsteady and steady states of thermophoretic natural convection in a Couette fluid flow in a vertical channel of two parallel vertical plates.

The aim of this study is to suggest how dust and particles can be filtered from the stratosphere by a 2-plated parallel-walled infinite rotatable, levitating vertical/horizontal channel (preferably) perforated with holes which have pockets on the cooler upper wall for collecting particles. A mathematical model is derived from Navier-Stokes equations of Momentum and energy and Concentration of species equation and numerical and analytical methods are suggested. This type of modelling can be cost-effective.

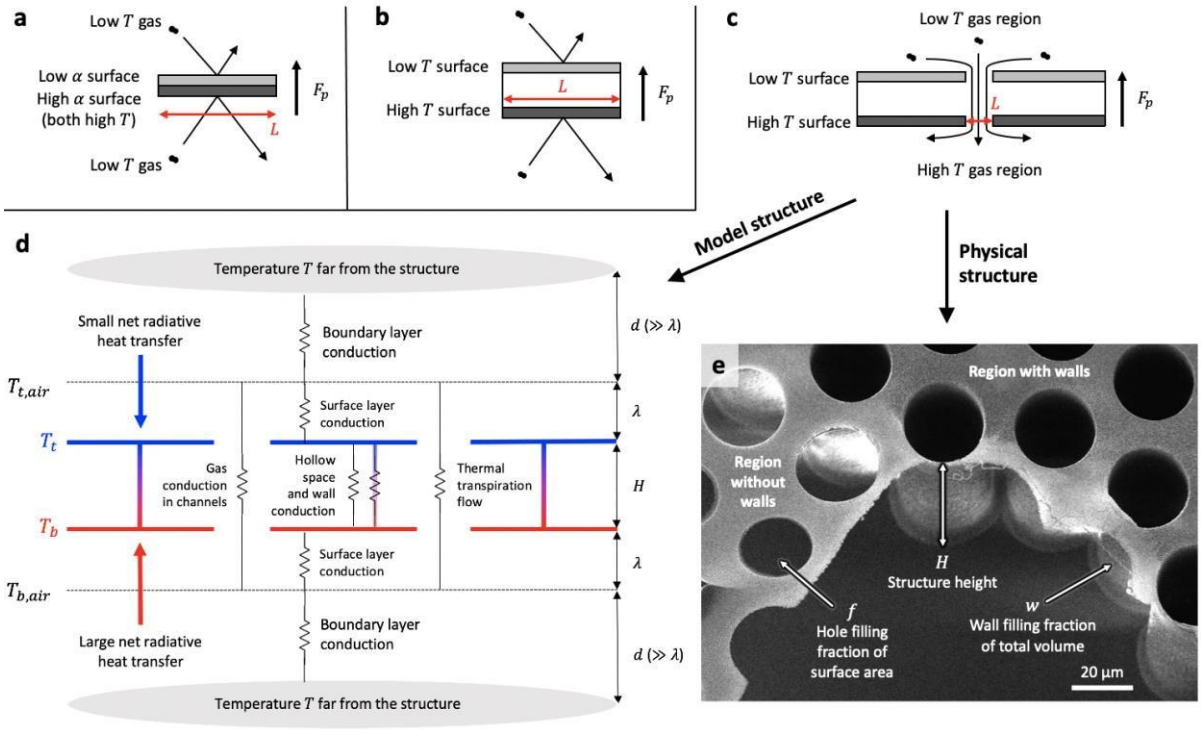

Figure 1a. The three photophoretic mechanisms which produce an upward lofting force on an object when a characteristic length scale L is less than the MFP (**a-c**) and physical and model structures that may produce a lofting force via thermal transpiration (**d** and **e**). **a** $\Delta\alpha$ photophoresis produced by a difference in α between the top and bottom surfaces of an isothermal structure that is warmer than the surrounding gas. **b** ΔT photophoresis produced by a difference in temperature between the top and bottom surfaces. **c** Thermal transpiration caused by the difference in

air temperature above and below the structure. In **a** and **b**, L is the minimumhorizontal dimension of the structure, whereas in **c** L is the horizontal dimension of the hole or channel. **d** SEM image of an example structure made of 100 nm thick alumina, showing the structure height H = 100 µm, wall filling fractions w = 0.006 in the region with walls and w =0 elsewhere, and hole filling fraction f = 0.4. Holes were not etched in bottom layer of the structure for clarity. The region with walls varies from our model structure because the walls are concentric with the holes, which reduces the local temperature gradient $T_b - T_t$ and the resulting thermal transpiration flow at each hole. **e** Generalized heat resistivity diagram for the 1D models. Each resistor represents a heat transfer term in the models. Source: Schafer, Kim, Vlassak and Keith (2023)

Description of Mathematical Problem

A typical model would be a one-dimensional analytical model representing a horizontally/vertically uniform bilayer structure with two infinitely thin, isothermal, perforated layers separated by a height L. The perforations have an area filling fraction, *f*, and the structural walls separating the layers have an area filling fraction w. The flow through the holes assumes they have dimensions much smaller than. At a distance from the structure equal to the thermal boundary layer thickness d, we assume the air has ambient temperature T'. The distance d is many orders of magnitude larger than λ in the quiescent stratosphere. Temperature at outer hot wall and outer cold wall are

$$T_{h,air} = T_h - \lambda \frac{T_h - T'}{d} \quad (1)$$

$$T_{c,air} = T_c - \lambda \frac{T_c - T'}{d} \quad (2)$$

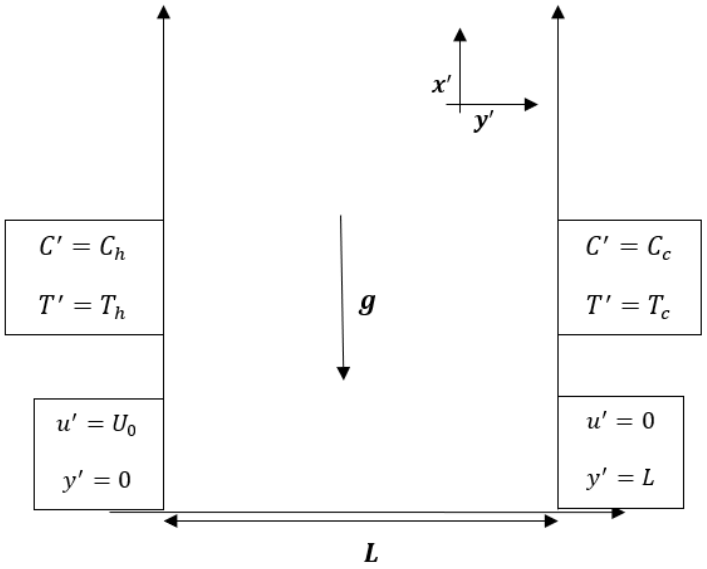

Figure 2: Systemic diagram of channel

We assume uniform pressure in channel, for simplicity we ignore holes and effects from holes and the boundary layer.

For a flow of a gaseous medium with particles in an alumina sandwich vertical/horizontal structure extremely long rectangular channel (two porous plates embedded in a porous medium) and shown schematically in Fig. 1b, where x'-axis pointing upwards along a channel of length ∞, in parallel with vectors of velocity and acceleration due to gravity in the other direction $\mathbf{v}(u', v')$ and $-\boldsymbol{g}$, this is necessary if all but the vector u' is required to disappear. The y'-axis is hence orthogonal to walls positioned at $y' = 0$ and $y' = L$ meaning they are distance L apart. If the flow is fully developed in the horizontal axis, we assume$v' = 0$, meaning there are no changes in velocity and dynamic pressure across channel while concentration and temperature are constant along the channel walls. At $t' \leq 0$, the two channel walls are expected to be resting and have the same temperature as the fluid which is T_0. At time $t' > 0$, channel wall temperature at $y' = 0$ rises to T_h leaving one hot and one cold wall T_c with a temperature difference defined by $\Delta T = T_h - T_c$. The presence of particles in the fluid with this temperature difference causes a free convective thermophoretic flow. Under the usual Boussinesq approximation, we take the characteristic density ρ_0 and $\upsilon \coloneqq \mu/\rho_0$ is kinematic viscosity. Taking

$$\beta = -(1/\rho_0)(\rho - \rho_0/T - T_0)_{C,p=Const.} \quad \text{and} \quad \beta^* = -(1/\rho_0)(\rho - \rho_0/C - C_0)_{T,p=Const.} \quad (3)$$

The transport equations are:

$$\frac{\partial u'}{\partial t'} = g\beta(T'-T_0) + g\beta^*(C'-C_0) + \upsilon_0\frac{\partial u'}{\partial y'} + \upsilon\left(\frac{\partial^2 u'}{\partial y'^2} - \frac{u'}{K_p}\right) - \frac{1}{\rho_0}\frac{\partial \mathrm{p}}{\partial \mathrm{x}} \quad (4)$$

$$\frac{\partial T'}{\partial t'} = \frac{k_f}{c_p\rho}\frac{\partial^2 T'}{\partial y'^2} + \frac{16\sigma_1 {T_0}^3}{3c_p\rho\chi}\frac{\partial^2 T'}{\partial y'^2} + \upsilon_0\frac{\partial T'}{\partial y'} \quad (5)$$

$$\frac{\partial C'}{\partial t'} = D\frac{\partial^2 C'}{\partial y'^2} - \frac{\partial}{\partial y'}(v_T + v_{PH})C' + \upsilon_0\frac{\partial C'}{\partial y'} \quad (6)$$

The initial and no slip boundary conditions in dimensionless form are:

$$t' \le 0: \; u' = 0,\; T' = T_0,\; C' = C_0 \text{ for } 0 \le y' \le L$$

$$t' > 0: \begin{cases} u' = 0; -k_f\frac{\partial T'}{\partial y'}\Big|_{y'=0} = h_1[T_h - T'(0)], \; C' = C_h \;\; at\; y' = 0 \\ u' = 0; -k_f\frac{\partial T'}{\partial y'}\Big|_{y'=L} = h_2[T'(L) - T_c], \; C' = C_c \;\; at\; y' = L \end{cases} \quad (7)$$

The first, second, third, fourth and terms on the RHS of the equation (4) denote the convection term related to temperature, convection term related to concentration, plate suction, porosity and pressure gradient. β, β^* are thermal and concentration volumetric expansion coefficients and c_p is specific heat at constant pressure. k_f denotes thermal conductivity coefficient while $h_1$and h_2 are

If ρ is the fluid density, σ_1 is the Stefan-Boltzmann constant, χ is the mean absorption coefficient, K_p is the porous medium, υ_0 is plate surface suction velocity, thermophoresis velocity v_T is directly proportional to temperature gradient and inversely proportional to kinematic viscosity of fluid.

The Talbot-Cheng-Schefer-Willis thermophoretic deposition velocity in the y-direction given has the form:

$$v_T = -k\frac{\upsilon}{T'}\frac{dT'}{dy} \quad (8)$$

The Loesche-Husmann photophoretic velocity is:

$$v_{PH} = -\frac{2}{3}\kappa_s\frac{\eta_{dyn}}{\rho\bar{T}r_0}\frac{IJ_1}{\frac{k}{r_0}+2\frac{k_g}{r_0}+4\sigma_{SB}\varepsilon {T_{bb}}^3}\boldsymbol{e}_z \quad (9)$$

r_0, κ_s, η_{dyn}, J_1, T_{bb},$\bar{T}$, k, k_g, σ_{SB}, ε and $\boldsymbol{e}_z$ are radius of particle, thermal creep coefficient, dynamic viscosity of gas, asymmetry factor and the additional radiative term $4\sigma_{SB}\varepsilon {T_{bb}}^3$and velocity coefficient $\boldsymbol{e}_z$.

Describing the volumetric flow rate which is equal to the bulk velocity is needed to obtain the pressure gradient

$$Q = \int_0^L u'dy \quad (10)$$

for simplicity we ignore holes and effects from holes, porosity, the boundary layer and unsteadiness. The transport equations then are:

$$g\beta(T'-T_0) + g\beta^*(C'-C_0) + \upsilon\left(\frac{\partial^2 u'}{\partial y'^2}\right) - \frac{1}{\rho_0}\frac{\partial \mathrm{p}}{\partial \mathrm{x}} = 0 \quad (11)$$

$$\frac{k_f}{c_p\rho}\frac{\partial^2 T'}{\partial y'^2} + \frac{16\sigma_1 {T_0}^3}{3c_p\rho\chi}\frac{\partial^2 T'}{\partial y'^2} = 0 \quad (12)$$

$$D\frac{\partial^2 C'}{\partial y'^2} - \frac{\partial}{\partial y'}(v_T + v_{PH})C' = 0 \quad (13)$$

for the following dimensionless quantities in equation

$$y = \frac{y'}{L},\; u = \frac{u'}{u_0}, u_0 = \frac{Q}{L},\; \theta = \frac{T'-T_0}{T_h-T_c},\; \phi = \frac{C'-C_0}{C_h-C_c},$$

$$N_t = \frac{T_0}{T_h-T_c}, N_c = \frac{C_0}{C_h-C_c}, T_0 = (T_h+T_c)/2,$$

$$C_0 = (C_h+C_c)/2,\; Bi_1 = \frac{h_1 L}{k_f},\; Bi_2 = \frac{h_2 L}{k_f} \quad (14)$$

and

$$Pr = \frac{c_p\mu}{k},\; Sc = \frac{\upsilon}{D},\; \alpha = \frac{L^2}{\mu u_0}\frac{\partial \mathrm{p}}{\partial \mathrm{x}},\; Gr = \frac{g\beta L^3(T_h-T_c)}{\upsilon^2},$$

$$Re = \frac{u_0 L}{\upsilon},\; t = \frac{t'\upsilon}{L^2},\; V_T = \frac{L}{\upsilon}v_T,\; Nr = \frac{16\sigma_1 {T_0}^3}{3c_p\rho\chi}\frac{\partial^2 T'}{\partial y'^2},$$

$$\lambda = \frac{Gr}{Re} = \frac{g\beta L^2(T_h-T_c)}{\upsilon u_0},\; b = \frac{\beta^*(C_h-C_c)}{\beta(T_h-T_c)},$$

$$C_{ph} = \kappa_s\frac{\eta_{dyn}}{\rho\bar{T}r_0}\frac{IJ_1}{\frac{k}{r_0}+2\frac{k_g}{r_0}+4\sigma_{SB}\varepsilon {T_{bb}}^3}\boldsymbol{e}_z \quad (15)$$

If $k\upsilon$ here represents the thermophoretic diffusivity then equation (8) and (9) can be written in the dimensionless form as:

$$V_t = -\frac{k}{(\theta+N_t)}\frac{d\theta}{dy} \text{ and } \int_0^1 udy = 1 \quad (16)$$

$$V_{ph} = -\frac{2}{3}c_{ph} \quad (17)$$

Closed form solutions

The equations (4) – (6) simplified, nondimensionalized can be rewritten in the following closed form:

$$\frac{\partial^2 u}{\partial y^2} + \lambda(\theta + b\phi) - \alpha = 0 \quad (18)$$

$$\frac{\partial^2 \theta}{\partial y^2}\left(\frac{1}{Pr} + Nr\right) = 0 \quad (19)$$

$$\frac{\partial^2 \phi}{\partial y^2} + Sc\left(k + \frac{2}{3}c_{ph}\right)\frac{\partial}{\partial y}\left[\frac{\phi+N_c}{\theta+N_t}\frac{\partial \theta}{\partial y}\right] = 0 \quad (20)$$

The boundary conditions are

$$t \le 0: \; u = 0,\; \theta = 0,\; \phi = 0 \text{ for } 0 \le y \le 1$$

$$t > 0: \begin{cases} u = 0, \frac{d\theta}{dy}\Big|_{y=0} = Bi_1\left[\theta(0) - \frac{1}{2}\right] \quad , \phi = \frac{1}{2} \; at\; y = 0 \\ u = 0, \frac{d\theta}{dy}\Big|_{y=1} = -Bi_2\left[\theta(1) + \frac{1}{2}\right], \phi = -\frac{1}{2} \; at\; y = 1 \end{cases} \quad (21)$$

by letting $a = \left(k + \frac{2}{3}c_{ph}\right)Sc$ and $z = N_t + \frac{1}{2} - y$ (See Magyari [24]). The solutions for the energy, concentration and momentum equations are given as we uniform pressure in channel,

With pressure gradient obtained from dimensionless volumetric flow rate $\int_0^1 udy = 1$

$$\theta(y) = d_1 y + d_2 \quad (22)$$

$$\phi(y) = K_2(d_1 y + d_2 + N_t)^{-a} - N_c - \frac{K_1}{d_1}\frac{(d_1 y + d_2 + N_t)}{(a+1)} \quad (23)$$

$$u(y) = \frac{1}{{d_1}^2}\Big[K_4 + K_3(d_1 y + d_2 + N_t) - K_2 b\frac{(d_1 y + d_2 + N_t)^{2-a}}{(1-a)(2-a)} + (N_t + bN_c)\frac{(d_1 y + d_2 + N_t)^2}{2} - \left(1 + \frac{K_1 b}{d_1(a+1)}\right)\frac{(d_1 y + d_2 + N_t)^3}{6}\Big] \quad (24)$$

K_1...K_4 are all constants given in the Appendix

$$\alpha = -12 + \lambda\left[12b_4 + \frac{3b_1(4Nt^2-1)+2b_2Nt(1-4Nt^2)-b_2(12Nt^2+1)+24(b_3b_5-b_3b_6+b_1Nt^2)}{2}\right] \quad (25)$$

is the pressure gradient in the channel

If $z_0 = N_t + \frac{1}{2}$ and $z_1 = N_t - \frac{1}{2}$, then $b_1 \ldots, b_6$ are given in the Appendix

Numerical Solutions

We use a standard finite approach proposed by Langtangen [30] with the THOMAS algorithm for tridiagonal systems to discretize the term $D_y C D_y \theta$ in (20) and the equations (11) - (13) in the second order approximations centred-at-space to our spatial derivatives, using the backwards difference approximations for time derivatives of the second order hence ensuring that $\Delta t \approx (\Delta y)^2$ on FORTRAN 95.

We call on the Thomas algorithm to invert the tridiagonal matrices. These processes continue until a steady state value is reached that observes the convergence criterion $\frac{\sum|A_{i,j+1}-A_{i,j}|}{(I-1)|A|_{max}} < 10^{-5}$

RESULTS AND DISCUSSION

The values of $Sc = 0.6$ (fog) and $Sc = 100$ (soot) was used in the study as approximated for values of diffusions of water vapor and dust particles respectively in air, Grosan *et al* (2009). Excluding when varying Sc and Pr. The effects of thermophoretic coefficient k are considered varying dimensionless time in steady and unsteady states. The value $k = 0$ suggests an absence of thermophoresis. λ is taken as -100 (or 100) which represents a opposing or aiding flow respectively. Through all the various profiles, $c_{ph} = 0$, $Bi_1 = Bi_2 = \infty$, $N_c = 2.0$, $N_t = 8.0$ are constant. $b = 1.0$ occurs when $\beta(T' - T_0) = \beta^*(C' - C_0)$ that is when the thermal buoyancy and the buoyancy effect due to concentration gradients are both equal and aid each other (positive).

Velocity Profiles

We firstly consider two practical situations: Figure 3(a) depicts the absence of thermophoretic effects on transient and steady state velocity profile (at $Sc = 0.6$) for an opposing flow ($\lambda = -100$) with normal concentration of particles at normal room temperature. 3(b) displays effect of thermophoresis on velocity when $k = 2.0$ with the above conditions. When time increases so does velocity but thermophoretic effect is negligible in the transient state velocity of water vapor particles ($Sc = 0.6$), with diameter $1 < D_p \leq 10\mu m$. We Secondly consider two similar situations: 3(c) In the absence of thermophoretic effects (and $Sc = 0.6$) for an aiding flow ($\lambda = 100$) and 3(d) In the presence of thermophoresis ($k = 2.0$) when time is varied in the velocity profiles. These Figures reveal, as time passes, the fluid velocity continues to improve and aims for a steady state. Which can be explained by the effect temperature has on convection currents and hence on kinetic energy and therefore velocity of fluid. These figures also display reversed direction of flows in aiding and opposing flows when buoyancy effects are dominant as in Sasse *et al* (1994). Figure 3(e) exhibits the effects of buoyancy ratio on velocity profile at $k = 1.2$, $Sc = 100$ and $t = 0.05$ taking the buoyancy ratio at $b = -1, 0, 5, 10$ consistent with Postelnicu (2007) . At $b = -1$, we observe a drop in velocity in the vicinity of the cold plate is much lower than the increment in velocity at the hot boundary, profile exhibits a case when the two buoyant mechanisms of thermal buoyancy and concentration gradients oppose each other. The velocity profile at $b = 5$ and $b = 10$ shows a drastic rise of velocity at the hot boundary and a fall of velocity in the vicinity of the cold plate, this is due to increase in surface heat at the hot plate and mass transfer rates. Figure 3(f) illustrates the velocity profiles for different values of the Schmidt number. Obviously, the maximum value of velocity profiles at the hot plate is greater than the absolute minimum value of the velocity profiles at the cold plate. Increase in Schmidt number drops the velocity. Figures 3(g), 3(h), 3(i) display effects of Prandtl number, mixed convection parameter and thermophoretic coefficient on velocity profile across the channel.

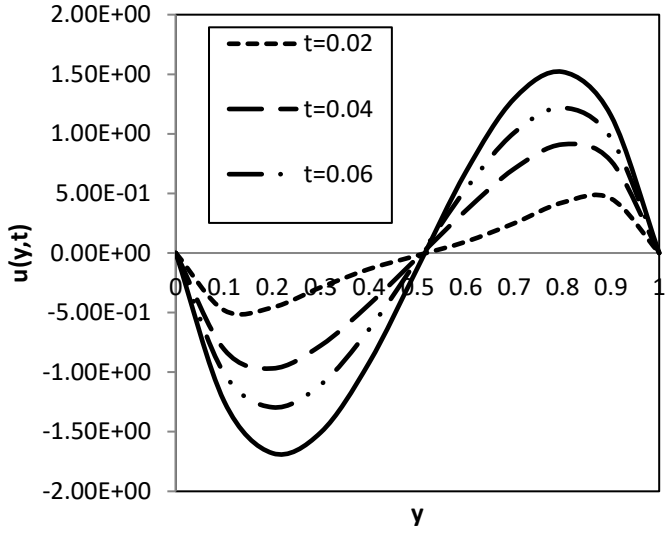

Figure 3a: Velocity profile in absence of thermophoresis $(k = 0, c_{ph} = 0, Pr = 0.71, Sc = 0.6, b = 1.0, N_c = 2.0,\ N_t = 8.0, \alpha = 1.0, \lambda = -100\ , Bi_1 = Bi_2 = \infty,)$

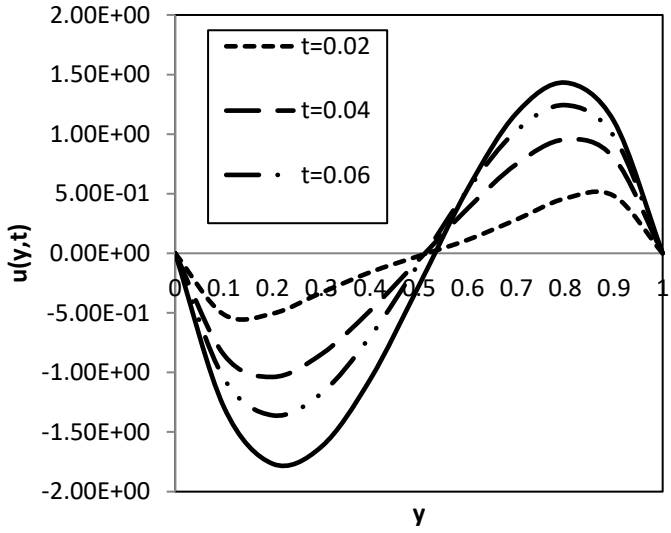

Figure 3b: Velocity profile in the presence of thermophoresis $(k = 2.0, c_{ph} = 0, Pr = 0.71, Sc = 0.6, b = 1.0, N_c = 2.0, N_t = 8.0, \alpha = 1.0, \lambda = -100, Bi_1 = Bi_2 = \infty,\ )$

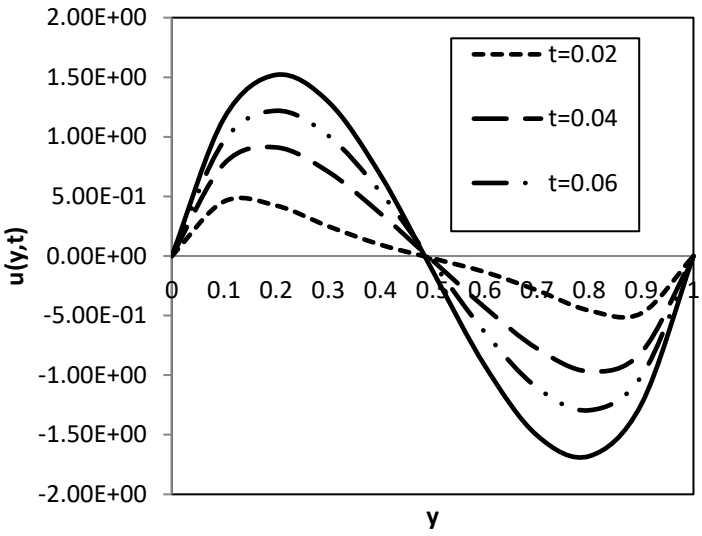

Figure 3c: Velocity profile for $(k = 0, c_{ph} = 0, Pr = 0.71, Sc = 0.6, b = 1.0, N_c = 2.0,\ N_t = 8.0, \alpha = 1.0, \lambda = 100\ , Bi_1 = Bi_2 = \infty,\ )$

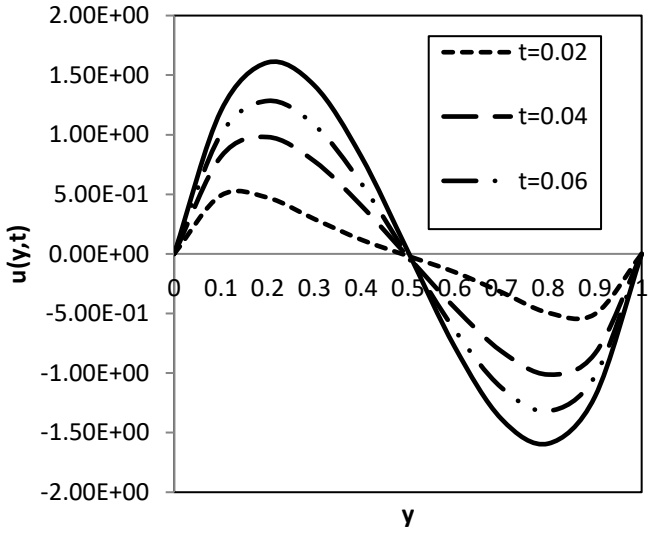

Figure 3d: Velocity profile for $(k = 2.0, c_{ph} = 0, Pr = 0.71, Sc = 0.6, b = 1.0, N_c = 2.0,\ N_t = 8.0, \alpha = 1.0, \lambda = 100, Bi_1 = Bi_2 = \infty,\ )$

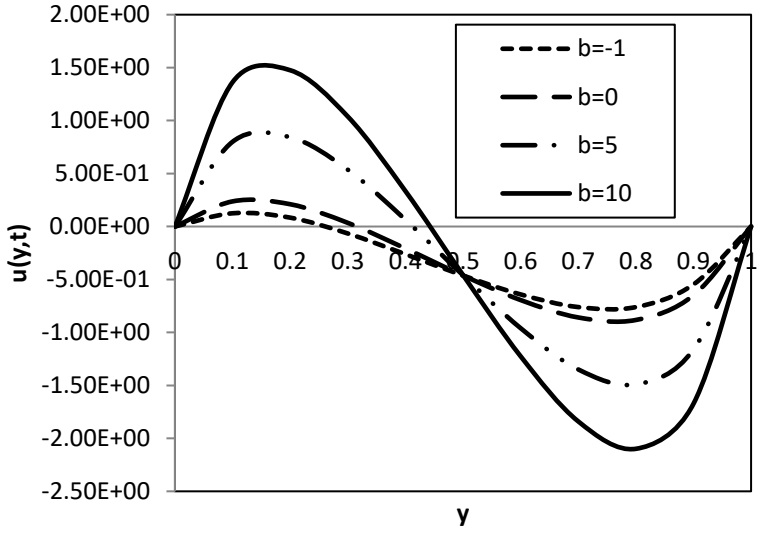

Figure 3e: Velocity profile for $(k = 1.2, c_{ph} = 0, \alpha = 10, t = 0.05, Pr = 0.71, Sc = 100, N_c = 2.0,\ N_t = 8.0, \lambda = 100, Bi_1 = Bi_2 = \infty,\ )$

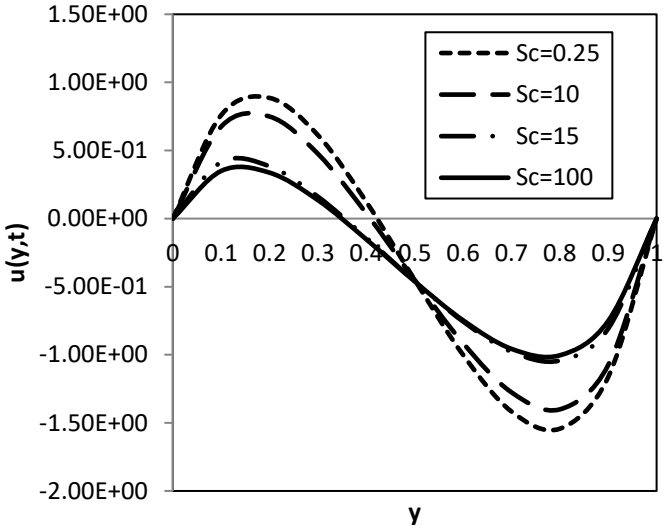

Figure 3f: Velocity profile for $(k = 1.2, c_{ph} = 0, \alpha = 10, t = 0.05, Pr = 0.71, b = 1.0, N_c = 2.0,\ N_t = 8.0, \lambda = 100\ , Bi_1 = Bi_2 = \infty,\ )$

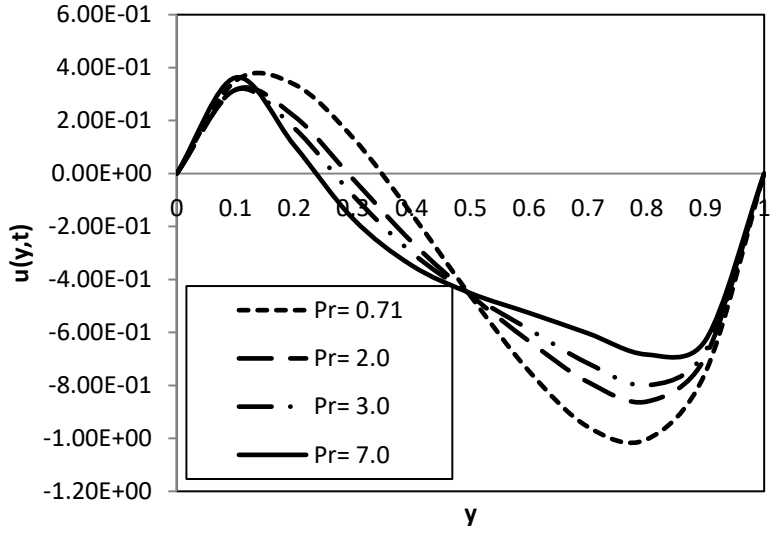

Figure 3g: Velocity profile for $\left(k = 1.2, c_{ph} = 0, \alpha = 10, t = 0.05, Sc = 100, b = 1.0, N_c = 2.0,\ N_t = 8.0, \lambda = 100, Bi_1 = Bi_2 = \infty,\ \right)$

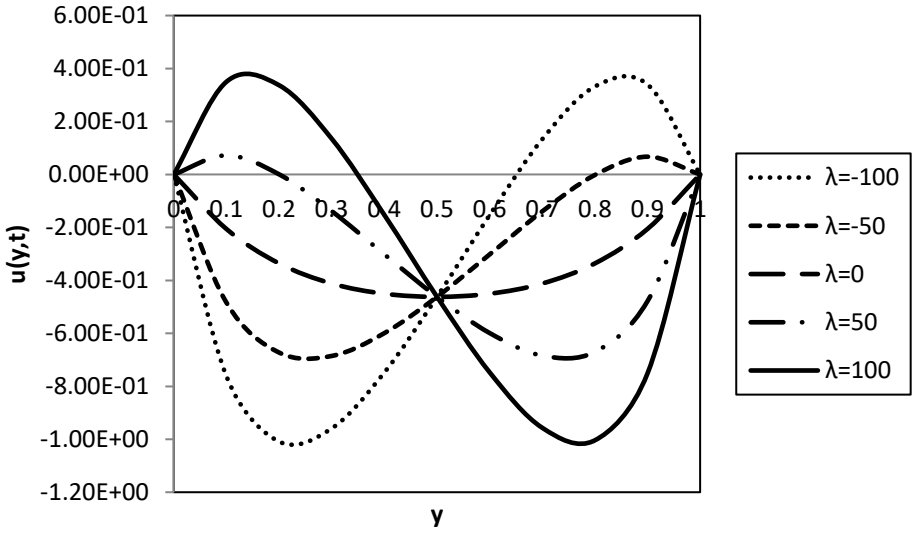

Figure 3h: Velocity profile for various values of the mixed convection (or buoyancy) parameter
$\left(k = 1.2, c_{ph} = 0, t = 0.05, Sc = 100, Pr = 0.71, b = 1.0, N_c = 2.0,\ N_t = 8.0, \alpha = 10, Bi_1 = Bi_2 = \infty,\ \right)$

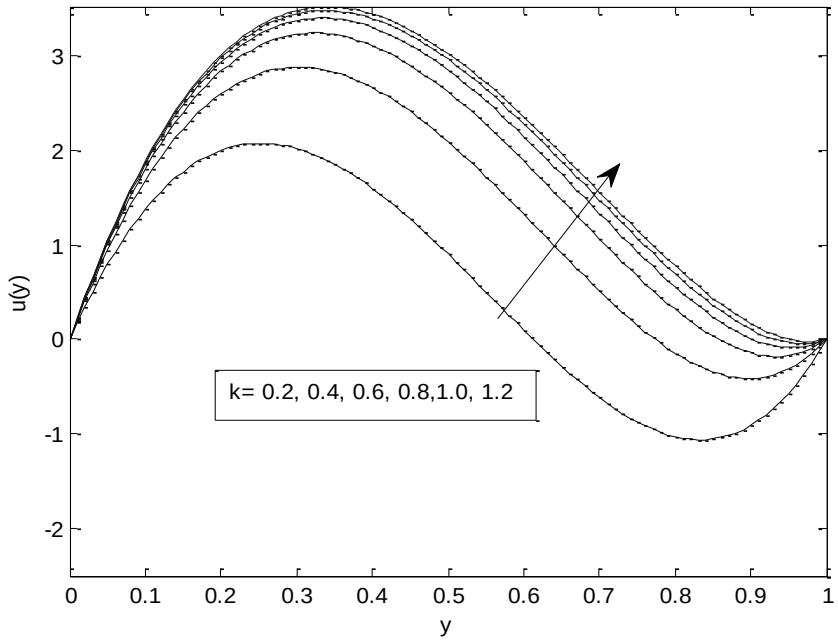

Figure 3i: Steady state velocity profile for various values of the thermophoretic coefficient
$(\alpha = 10, c_{ph} = 0, Sc = 100, Pr = 0.71, b = 1.0, N_c = 2.0,\ N_t = 8.0, \lambda = 100, Bi_1 = Bi_2 = \infty,\ )$

Particle Concentration Profiles

Figure 4(a) depicts the absence of thermophoretic effects on transient $t = 0.002, 0.004, 0.006$ and steady state concentration profile (at $Sc = 0.6$) with normal concentration of particles at normal room temperature. 4(b) shows the effect of thermophoresis on transient and steady state concentration ($k = 2.0$) with the same above conditions. Thermophoresis has no significant effect on concentration of water vapor particles ($Sc = 0.6$). Figure 4(c) considers a concentration profile of particles with thermophoretic effects (at $k = 1.2$) varying the Schmidt number ($t = 0.05$). We observe a symmetric graph with midchannel $at\ y = 0.5$. Schmidt number is shown to decrease concentration. 4(d) displays an enhancement in concentration as Pr increases (at time 0.05). This graph depicts an additional rise in concentration in the vicinity of the hot plate for dust particles ($Sc = 100$) suspended in water ($Pr = 0.71$) and a drop at the cold plate. In addition, it can be seen that particles suspended in water have $\phi(y) = 0$ at $0.3 < y < 0.7$ while those suspended in a gaseous medium ($Pr = 0.71, 2.0, 3.0$) have $\phi(y) = 0$ at the channel midcentre. Figure 4(e) shows that in steady state, the thermophoretic coefficient k enhances concentration for ($Sc = 100$) at steady state. These results are consistent with Tsai & Lu (1995)

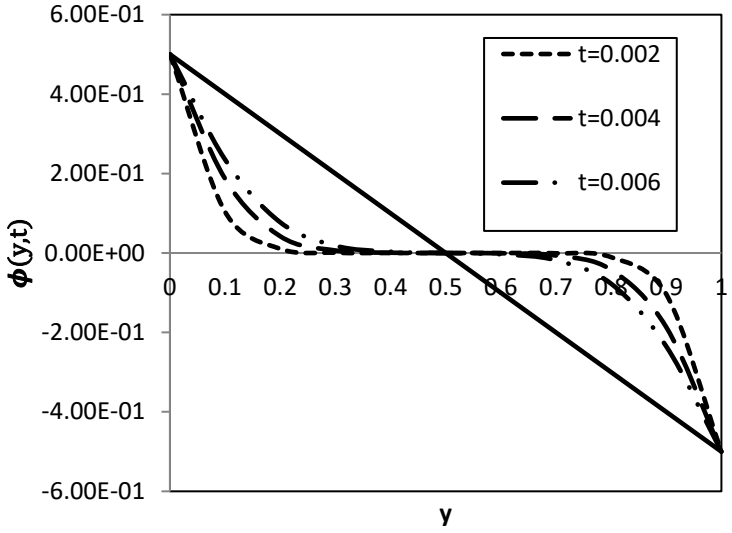

Figure 4a: Concentration profile for $(k = 0, c_{ph} = 0, Pr = 0.71, Sc = 0.6, N_c = 2.0,\ N_t = 8.0, Bi_1 = Bi_2 = \infty,\ )$

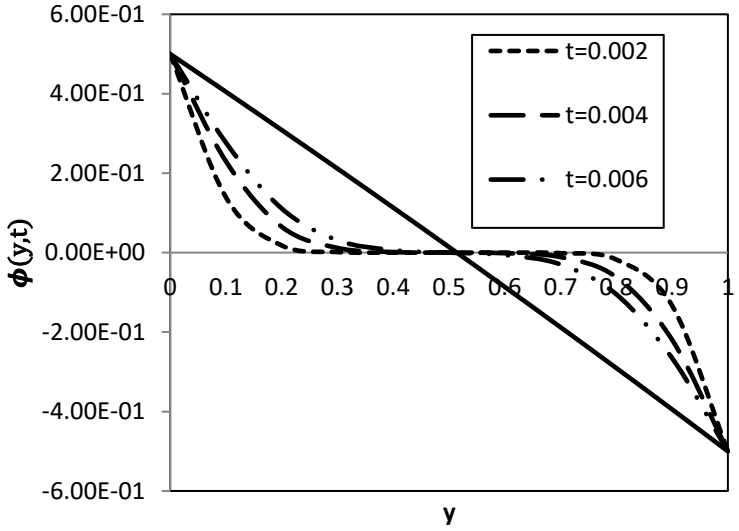

Figure 4b: Concentration profile for $(k = 2.0, c_{ph} = 0, Pr = 0.71, Sc = 0.6, N_c = 2.0, N_t = 8.0, Bi_1 = Bi_2 = \infty,\ )$

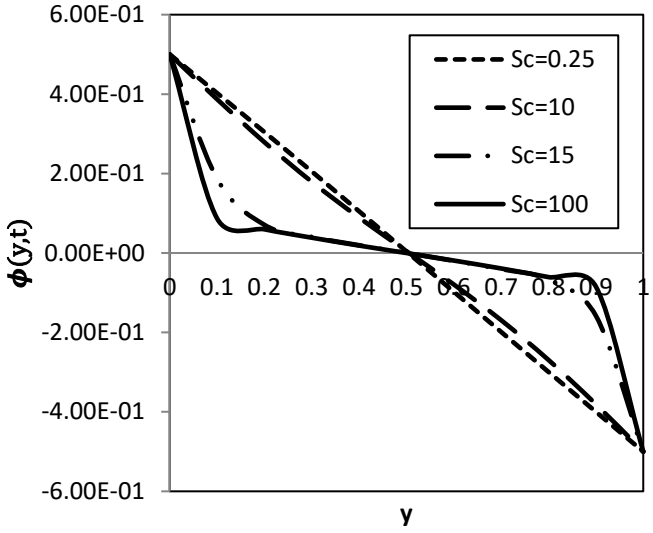

Figure 4c: Concentration profile for different values of the schmidt number $(k = 1.2, Pr = 0.71, c_{ph} = 0,\ t = 0.05, N_c = 2.0, N_t = 8.0, Bi_1 = Bi_2 = \infty,\ )$

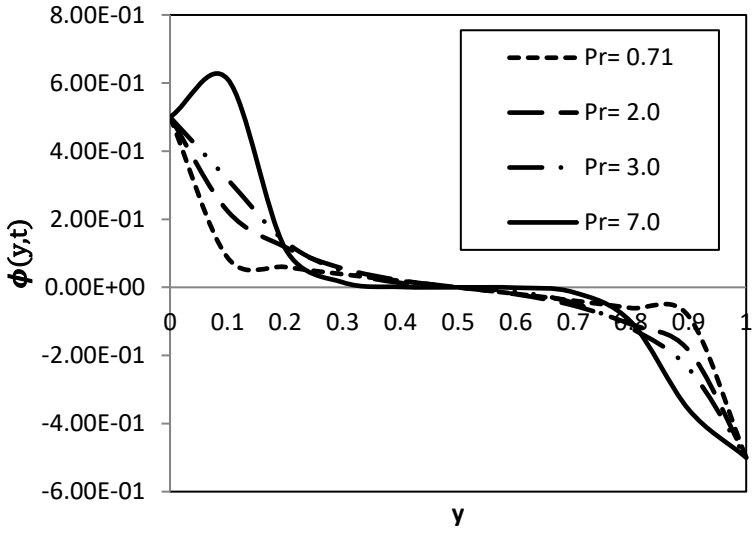

Figure 4d: Concentration profile for different values of Prandtl number $(k = 1.2, c_{ph} = 0, Sc = 100, t = 0.05, N_c = 2.0, N_t = 8.0, Bi_1 = Bi_2 = \infty,\ )$

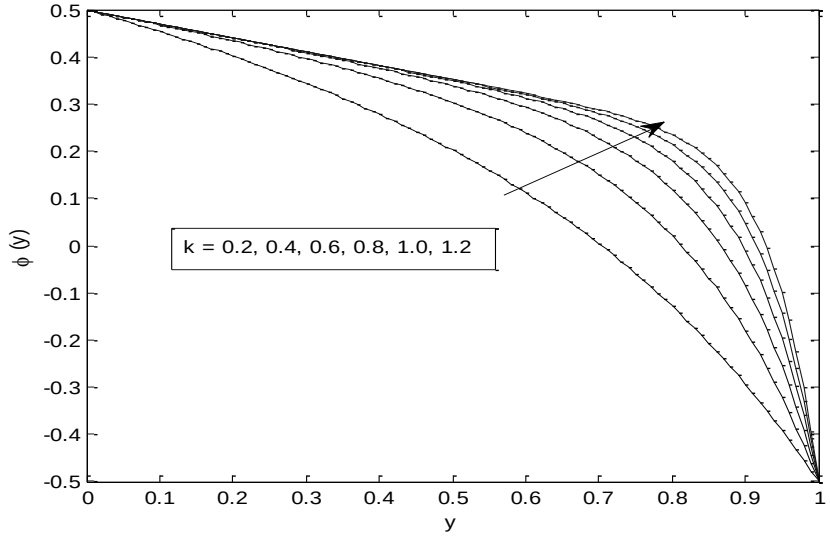

Figure 4e: Concentration profile for different values of thermophoretic coefficient $(Sc = 100, N_c = 2.0, N_t = 8.0, Bi_1 = Bi_2 = \infty,\ )$

Table 1 displays the values for velocity at time $t = 0.8$ across the channel for different values of y. Table 2 displays values for concentration at time $t = 0.4$. For two values of k, $k = 0$ and $k = 2.0$ comparing values with two methods. Table 1 also shows that exact values are slightly higher than those obtained from Finite Difference Scheme for $y = 0.2$ only. Table 2 shows that this is also true for Concentration when there is thermophoresis. Table 1 and 2 show that Velocity and concentration reduces across the channel.

Table 1: Comparison of numerical value of the transient state velocity obtained using the implicit finite difference at $t = 0.8$ and the steady state velocity obtained analytically when λ=100, $c_{ph} = 0$, α =10.0, Pr = 0.71, b=1.0, Sc = 0.6, $Bi_1 = Bi_2 = \infty$, N_c= 2.0 and N_t= 8.0

	$k = 0$		$k = 2.0$	
y	**Implicit finite difference**	**Analytical method**	**Implicit finite difference**	**Analytical method**
0.2	0.800007	0.80028	0.886163	0.886373
0.4	-0.40000	-0.39956	-0.26097	-0.26063
0.6	-2.00000	-1.99957	-1.85995	-1.85961
0.8	-2.40001	-2.39974	-2.31208	-2.31187

Table 2: Comparison of numerical value of the transient state concentration obtained using the implicit finite difference at $t = 0.4$ and the steady state concentration obtained analytically when $c_{ph} = 0$, Pr = 0.71, Sc = 0.6, $Bi_1 = Bi_2 = \infty$, N_c= 2.0 and N_t= 8.0

	$k = 0$		$k = 2.0$	
y	**Implicit finite difference**	**Analytical method**	**Implicit finite difference**	**Analytical method**
0.2	0.300002	0.300002	0.308646	0.308652
0.4	0.100001	0.100001	0.113307	0.113317
0.6	-0.100000	-0.100000	-0.08634	-0.08633
0.8	-0.300000	-0.300000	-0.29064	-0.29063

CONCLUSION

The important findings from graphical results show comparisons between pairs of different practical situations: (i) without thermophoresis and with thermophoresis (ii) for $Sc = 0.6$ (water vapor) and $Sc = 100$ (dust particles) (iii) for aiding and opposing flows. These findings reveal that thermophoresis has no appreciable effect on velocity and concentration for $Sc = 0.6$, hence water vapor particles do not need thermophoretic effect to move; fluid velocity is

improved with increments in time until steady conditions are achieved. With aiding and opposing flows, the direction of flows is reversed; Schmidt number and Prandtl number drops thermophoretic velocity and finally thermophoresis has appreciable increase on steady state velocity for $Sc = 100$.

REFERENCES

Al-Amri, F. G. (2021). Fully developed nanofluid mixed convection flow in a vertical channel, *Journal of Physics: Conference Series*, 829 (1) 012-018.

Barletta, A., Magyari & E., Keller, B. (2005). Dual mixed convection flows in a vertical channel, *International Journal of Heat and Mass transfer*, 48(23-24), 4835-4845.

Bouhdjar A. & Harhad A. (2002). Numerical analysis of transient mixed convection flow in storage tank: influence of fluid properties and aspect ratios on stratification. *Renewable Energ*, 25(4), 555 - 567.

Das, S., Jana, R. N. & Makinde, O. D. (2016). Transient Natural convection in a vertical channel filled with nanofluids in the presence of thermal radiation. *Alexandria Engineering Journal*, 55(1), 253-262.

Epstein, M., Hauser, G.M. & Henry, R.E. (1985). Thermophoretic deposition of particles in natural convection flow from a vertical plate. *ASME Journal of Heat and Transfer*, 107 (1985) 21-37.

Flagan, R. C. & Seinfeld, J. H. (1988). FUNDAMENTALS OF AIR POLLUTION ENGINEERING. Prentice-Hall, Inc. , Englewood Cliffs, New Jersey.

Grosan, T., Pop, R. & Pop, I. (2009). Thermophoretic deposition of particles in fully developed mixed convection flow in a parallel-plate vertical channel. *Heat and Mass Transf*er, 45, 503-509.

J

ayaraj, S. (1999). Finite difference modelling of natural convection flow with thermophoresis. *International Journal of Numerical Methods for heat and fluid flow*, 9(6), 692-704.

Jha, B. K. & Ajibade, A. O. (2010). Transient natural convection flow between vertical parallel plates: one plate isothermally heated and the other thermally insulated. *J. Process Mech Eng.* 224, Part E.

Jha, B. K. (2001). Natural Convection in unsteady MHD Couette flow. *Heat and Mass Transfer*, 37, (2001) 329-331.

Jha, B. K. & Sani, H. N. (2021). Thermophoresis on free convective unsteady/steady Couette fluid flow with mass transfer. *International Journal of Applied and Computational Mathematics*. **7** (80), (2021) DOI:10.1007/540819-021-00980-0

Karthikeyan, C.P., Kalpana, G., Krishnamoorthy, V. & Samuel, A. A. (2020). Transient numerical analysis of thermophoresis and particle dynamics in a nanofluid-pool boiling conditions. *Journal of Molecular Liquids*, 301, 112459.

Langtangen, H. P. (2003). *Computational Partial Difference equations: Numerical methods and Diffpack programming*. Springer, (2003) 459-491.

Magyari, E., (2009). Thermophoretic deposition of particles in fully developed mixed convection flow in a parallel-plate vertical channel. *Heat and Mass Transfer*, 45, 1473-1482.

Mensch, A. E. & Cleary, G.T. (2019). Measurements and Predictions of thermophoretic soot deposition, International Journal of Heat and Mass Transfer. 143, (2019) 1016.

Messerer, A., Niessner, R. & Pöschl, U. (2003). Thermophoretic deposition of soot aerosol particles under experimental conditions relevant for modern diesel engine exhaust gas systems. *Journal of Aerosol Science*, 34 (8), 1009-1021.

Nguyen, C.T., Maïga, S. E. B., Maré, T. & Galanis N. (2004). Transient development of laminar mixed convection flow in a vertical tube. *WIT Press.*

Paul, T., Jha, B. K. & Singh, A. K. (1996). Transient free convective flow in a vertical channel
with constant temperature and constant heat flux. *Heat and Mass Transfer*, 32(1/2), 61 – 63.

Popa, C. V., Nguyen, C. T., Fohanno, S. & Polidiri G. (2014). Transient mixed convection flow of nanofluids in a vertical tube. *International Journal of Numerical methods for heat and fluid flow*, 24(2), 376-389.

Postelnicu, A. (2007). Effects of thermophoresis particle deposition in free convection boundary layer from a horizontal flat plate embedded in a porous medium. *International Journal of Heat and Mass Transfer*, 50, 2981-298.

Rahman, M.M. & Carey, V. P. (1986). Steady and transient mixed convection near a vertical uniformly heated surface exposed to horizontal fluid flow. *Numerical Heat Transfer*, 10(4), 327 - 347.

Saleh, H., Hashim, I. & Basriati, S. (2013). Flow reversal of fully developed mixed convection in a vertical channel with chemical reaction, *International Journal of Chemical Engineering*. Article ID 310273 (2013) 4 pages, Hindawi.

Sasse, A.G.B.M., Nazaroff, W.W. & Gadgil, A. J. (1994). Particle filter based on thermophoretic deposition from natural convection flow. *Aerosol Science and Technology*, 20 (3), 227-238.

Singh, A. K., Gholami, H. R. & Soundalgekar,V. M. (1996). Transient free convection flow between two vertical parallel plates. *Heat and Mass Transfer*, 31, 329 - 331.

Sun, H., Li, R., Chénier E. & Lauriat, G. (2012). On the modeling of aiding mixed convection in vertical channels. *Heat Mass transfer*, 48(7), 1125-1134.

Talbot, L., Cheng, R.K., Schefer, R.W. & Willis, D.R. (1980). Thermophoresis of particles in a heated boundary layer. *J. Fluid Mech*. 101 (4), 737–758.

Tebbe, P. A. & Thiebeault, C. (2011). NUMERICAL TREATMENT OF THERMOPHORETIC DEPOSITION IN TUBE FLOW. *Slideplayer.com/slide/8255641*.

Tsai, C.-J. & Lu, H.-C. (1995). Design and Evaluation of a plate-to-plate thermphoretic precipitator, *Aerosol Science and Technology*. 22 (2), 172-180.

Wang, C.-C. & Chen, C.-K. (2006). Thermophoresis deposition of particles from a boundary layer flow onto a continuosly moving wavy surface. *Acta Mechanica*, 181, 139-151.

Xu, H. & Pop I. (2012). Fully developed mixed convection flow in a vertical channel filled with nanofluids, *Heat Transfer*. 39(8), 1086-1092.

APPENDIX A

$$K_1 = \frac{d_1}{2}(a+1)\left[\frac{(d_2+N_t)^a(1+2N_c)-(d_1+d_2+N_t)^a(2N_c-1)}{(d_2+N_t)^{a+1}-(d_1+d_2+N_t)^{a+1}}\right]$$

$$K_2 = \frac{(d_2+N_t)^a(d_1+d_2+N_t)^a(N_t-N_c)}{(d_1+d_2+N_t)^{a+1}-(d_2+N_t)^{a+1}}$$

$$K_3 = \frac{1}{d_1}\left[N_t(N_t+bN_c)+\frac{K_2 b\left[\left(N_t-\frac{1}{2}\right)^{2-a}-\left(N_t+\frac{1}{2}\right)^{2-a}\right]}{(1-a)(2-a)}-\frac{(12Nt^2+1)}{24}\left(1+\frac{K_1 b}{d_1(a+1)}\right)\right]$$

$$K_4 = \frac{1}{d_1}\left[\frac{N_t(4Nt^2-1)}{12}\left(1+\frac{K_1 b}{d_1(a+1)}\right)+\frac{(1-4Nt^2)(N_t+bN_c)}{8}+\frac{K_2 b\left(\frac{1}{4}-Nt^2\right)\left[\left(N_t-\frac{1}{2}\right)^{1-a}-\left(N_t+\frac{1}{2}\right)^{1-a}\right]}{(1-a)(2-a)}\right]$$

$$d_1 = -\frac{Bi_1 Bi_2}{[Bi_1(1+Bi_2)+Bi_2]}$$

$$d_2 = \frac{1}{2}\frac{[Bi_1(1+Bi_2)-Bi_2]}{[Bi_1(1+Bi_2)+Bi_2]}$$